



# Investigating the Propagation of Multiple Hydraulic Fractures in Shale Oil Rocks Using Acoustic Emission

Shan Wu<sup>1</sup> · Ke Gao<sup>1</sup> · Xiaoqiong Wang<sup>2</sup> · Hongkui Ge<sup>2</sup> · Yushi Zou<sup>2</sup> · Xiaohuan Zhang<sup>2</sup>

Received: 13 December 2021 / Accepted: 2 June 2022

© The Author(s), under exclusive licence to Springer-Verlag GmbH Austria, part of Springer Nature 2022

## Abstract

The propagation of multiple fractures plays a significant role in the effectiveness of hydraulic stimulation in shale oil reservoirs. Previous studies reported that the laminations and bedding interface in shale oil rocks could influence the propagation of single hydraulic fracture. However, the propagation mechanism of multiple fractures in such rocks is still unclear. Here we use a true-triaxial experimental system, together with the acoustic emission (AE) monitoring system, to investigate the propagation of multiple fractures in shale oil reservoir rocks. The results show that the fracture interference started at the initiation stage seriously affects the propagation of multiple fractures. More clusters per stage could aggravate the fracture interference near the wellhead. The laminations and bedding interfaces are the main causes of fracture interference and could hinder the height of hydraulic fractures. Shear-type AE event signals the generation of fracture interference caused by the slip of bedding interface and the deflection of fractures induced by the laminations. The mechanism of fracture interference not only lies in stress shadow but also in the changes in fluid pressure caused by the high permeability of laminations and bedding interface. The experimental results provide basic and detailed data for studying hydraulic fracturing in shale oil reservoirs.

## Highlights

- True-triaxial experiment is conducted to investigate the propagation of multiple hydraulic fractures.
- Both the lamination and bedding interface influence multiple hydraulic fracture propagation.
- The AE monitoring indicates many shear-type fractures when fracture interference appears.

**Keywords** Multi-cluster fracturing · Multi-fracture propagation · Shear-type AE · Stress shadow · Layered shale

## List of Symbols

$f_{pf}$  Perforation friction  
 $\rho_s$  Density of the fluid  
 $n_p$  Number of perforations  
 $d_p$  Diameter of the perforation

$K_d$  Discharge coefficient  
 $S_M$  Cluster spacing or stage spacing in the experiment  
 $L_M$  Half-length of a fracture in the experiment  
 $S_F$  Cluster spacing or stage spacing in the field  
 $L_F$  Half-length of a fracture in the field  
 $D$  Stage spacing  
 $d$  Cluster spacing  
 $A$  Asymmetry distribution of AE events  
 $N$  Total number of AE events  
 $c$  Half of the fracture height  
 $p$  Net pressure in the hydraulic fracture

✉ Ke Gao  
gaok@sustech.edu.cn

Xiaoqiong Wang  
wxq4526@163.com

<sup>1</sup> Department of Earth and Space Sciences, Southern University of Science and Technology, Shenzhen 518055, Guangdong, China

<sup>2</sup> State Key Laboratory of Petroleum Resources and Prospecting, China University of Petroleum (Beijing), Beijing, China

## 1 Introduction

The shale oil reservoir of the Lucaogou formation in Xinjiang Province of China has few natural fractures but many laminations and bedding interfaces (Huo et al. 2019; Luo et al. 2018). The few natural fractures make it difficult to form complex fracture networks by hydraulic fracturing (Li et al. 2020). Therefore, multi-stage and multi-cluster techniques have to be employed to stimulate the reservoir (Luo et al. 2018). However, the growth of multiple fractures can be easily restrained when the stage-cluster spacing is too short (Manchanda et al. 2020). The immature development of multiple fractures is a problem caused by the interference of stress fields among multiple fractures. Previous numerical simulations by Wu and Olson (2015) indicated that the “stress shadow” produced by old fractures could significantly affect the propagation of new fractures, i.e., the so-called fracture interference. Although increasing the cluster spacing can be a direct solution to reduce fracture interference, excessive cluster spacing may lower the efficiency of hydraulic fracturing.

The optimization of cluster spacing could rely on the study of the propagation of multiple fractures. Numerical simulations have been applied to study the associated influencing factors, such as perforation friction, rock mechanical properties, and fracturing fluid viscosity (Liu et al. 2020a; Xiong et al. 2020). However, only a few numerical studies focus on the effect of the unique structures in shale oil rocks, such as the lamination and bedding interface. This is mainly limited by the difficulties in fabricating physical models containing laminations and bedding interfaces. The lamination is a structure-like lasagna consisting of thin layers of rock with different properties, and thus the rock containing this is heterogeneous and anisotropic. Yang et al. (2020) studied the influence of heterogeneity on multi-stage fracture propagation. However, the heterogeneity distribution characteristics in their models cannot reflect the anisotropy of laminations, which makes the results limited. The bedding interface is the interval of different layers of lamination and is usually closed under in-situ stress conditions. The numerical methods appropriate for such analysis should be able to handle the discrete parts in the intact rock for modeling bedding interfaces. Zou et al. (2017) established a layered model using the discrete element method and discussed the influence of the number and physical properties of bedding interface on hydraulic fracture propagation. However, the hydraulic fractures in their numerical simulations are merely planar, which cannot fully reflect the fracture interference caused by non-planar fractures. The field fracturing and experiments of the Lucaogou formation show that there are many non-planar fractures after hydraulic stimulation (Huo et al. 2019; Zhang et al. 2021a). To the best of our

knowledge, it is difficult to investigate the problem of multi-cluster fracture propagation under the influence of laminations and bedding interface by theoretical and numerical methods. Therefore, it is necessary to conduct laboratory experiments to thoroughly examine such fracture propagation mechanism in the Lucaogou formation.

The experiments on the propagation of multiple fractures are relatively rare. Previous experiments focus on the propagation of single fractures due to the limitation of experimental systems (Hou et al. 2014; Liu et al. 2018; Yuan et al. 2016). The condition of a single fracture is easy to set in experiments but gives only slight reference to multi-cluster fracturing in the field. Li et al. (2020) tried to use a multi-stage fracturing system to study the stimulation effect of different fluid types on shale oil rock in the condition of three stages (one cluster per stage). Zhang et al. (2021b) used more clusters in each stage and studied the different fracturing modes for stimulating multiple fractures in shales. In their experiment, CT scan imaging and tracer are used to describe the final shape of hydraulic fractures, in which the dynamic process of fracture propagation and the study of the properties of hydraulic fractures are missing (Hampton et al. 2014; Zou et al. 2016). In addition, their experiments are limited to revealing the mechanism of fracture interference. To obtain the propagation process and the mechanical properties of hydraulic fractures, acoustic emission (AE) monitoring is usually used together with true triaxial hydraulic fracturing experiments (Petružálek et al. 2020; Zhai et al. 2020). The localization and mechanical mechanism inversion of fractures based on AE events have been successfully applied to investigate the propagation mechanism of a single hydraulic fracture under the influence of bedding interface and natural fractures (Li et al. 2018a; Wu et al. 2019). To improve the understanding of the propagation of multiple fractures, AE monitoring could be further combined with the multi-stage fracturing system.

In this paper, we use a novel experimental process proposed by Zhang et al. (2021b) to investigate the propagation of multiple fractures in the Lucaogou shale reservoir and employ the AE technique to monitor the dynamic process of hydraulic fracturing. The location and properties of fractures inverted based on AE events are used to identify the characteristics of initiation and propagation of multi-clusters fractures and interpret the fracture interference in the Lucaogou formation (Ishida et al. 2017; Wu et al. 2019). The effect of the number of clusters per stage, bedding interface condition, injection rate, and fracturing mode are investigated in detail together with the injection pressure and the results of AE events. The paper is organized as follows. The samples, equipment, and procedures of the experiment are briefly introduced in Sect. 2. In Sect. 3, we overview the method used to analyze AE events and present the results from the analysis. Section 4 includes discussions of the characteristic

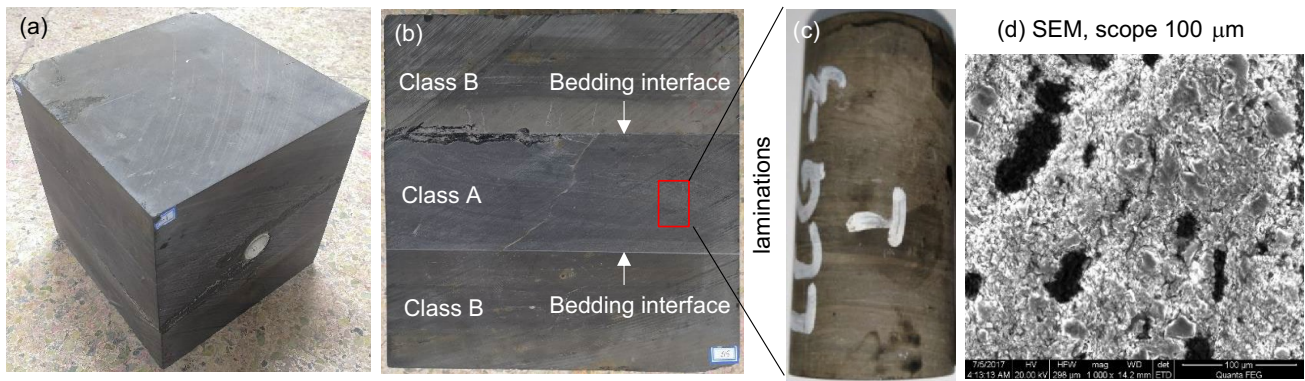


**Fig. 1** **a** Cubic sample with a size of 300 mm × 300 mm × 300 mm, and **b** structure of the sample. **c** Core of Lucaogou rock and **d** scanning electron microscope (SEM) image

of multi-cluster fracturing of the Lucaogou shale. The conclusions are drawn at the end.

## 2 Experimental Setups

### 2.1 Sample Preparation

The shale in the Lucaogou formation has well-developed beddings, and thus forms a series of structures including laminations and bedding interfaces (Li et al. 2020). The morphology of the Lucaogou shale is shown in Fig. 1a, which indicates obvious laminations in the core sample (Fig. 1c) and a straightforward directional structure arrangement in the scanning electron microscope (SEM) image (Fig. 1d). In this study, we collect two types of shale outcrops from the Lucaogou formation, and their main compositions are similar to those in the underground. As shown in Fig. 1b, the class A rock, with an average tensile strength of 9.7 MPa, is selected as the fracturing layers in the middle; while the class B rock, with an average tensile strength of 7.9 MPa, is chosen as the interlayers and placed outside the class A rock. The formed sandwich-shape cubic sample for the fracturing experiment is shown in Fig. 1a, b. We glue the class A and class B rocks together with epoxy resin to simulate the adhesion bedding interfaces with low permeability and high cohesive stress. For comparison, we also simply stack up the three rock blocks together in the same order but without gluing them to realize the non-adhesion bedding interfaces. Comparing the two types of bedding interfaces could help reveal the influence of bedding interface on multi-cluster fracturing.

For hydraulic fracturing, we use a uniform cluster spacing in the experiment, which is a standard setup in the field. Although the previous studies demonstrated that nonuniform cluster spacing could promote fracture growth (Wu et al. 2016), it is challenging to set nonuniform clusters in

the samples in laboratory experiments, and how the cluster spacing could promote fracture growth is out of the scope of current research. Therefore, to simplify the sample preparation, we set three fracturing zones as the three stages in each sample (Fig. 2a), and cut a series of notches with a depth of 2 mm around the circumference of the wellbore as clusters.

Flow resistance is a crucial factor in controlling the propagation of multiple fractures. The perforation friction in the field can adjust flow resistance. In our experiment, the cluster is created by notches rather than perforations. Therefore, the control of perforation friction could be regarded as controlling the cluster friction in each stage. The perforation friction is a function of perforation number, that is

$$f_{pt} = \frac{0.2369\rho_s}{n_p^2 d_p^4 K_d^2}, \quad (1)$$

where  $\rho_s$  is the density of the fluid,  $n_p$  is the number of perforations,  $d_p$  is the diameter of the perforation, and  $K_d$  is the discharge coefficient ranging from 0.56 to 0.89 (Bunger et al. 2014; Crump and Conway 1988; Lecampion and Desroches 2014; Wu et al. 2016). The cluster friction in each stage could be a function of the notch number. To study the multiple fracture propagation, we choose three different cluster numbers (i.e., 1, 3, and 5) with the same spacing in each stage and try to create an effective propagation of multiple fractures during the simultaneous fracturing. The stage spacing and cluster spacing are marked in Fig. 2b.

### 2.2 Apparatus and Experimental Procedures

We use a true triaxial fracturing simulation system developed by the China University of Petroleum (Beijing) to conduct the current experiments. The equipment can apply boundary forces from three orthogonal directions to simulate the underground in-situ stress conditions. The boundary loading acting in the vertical direction (i.e., perpendicular

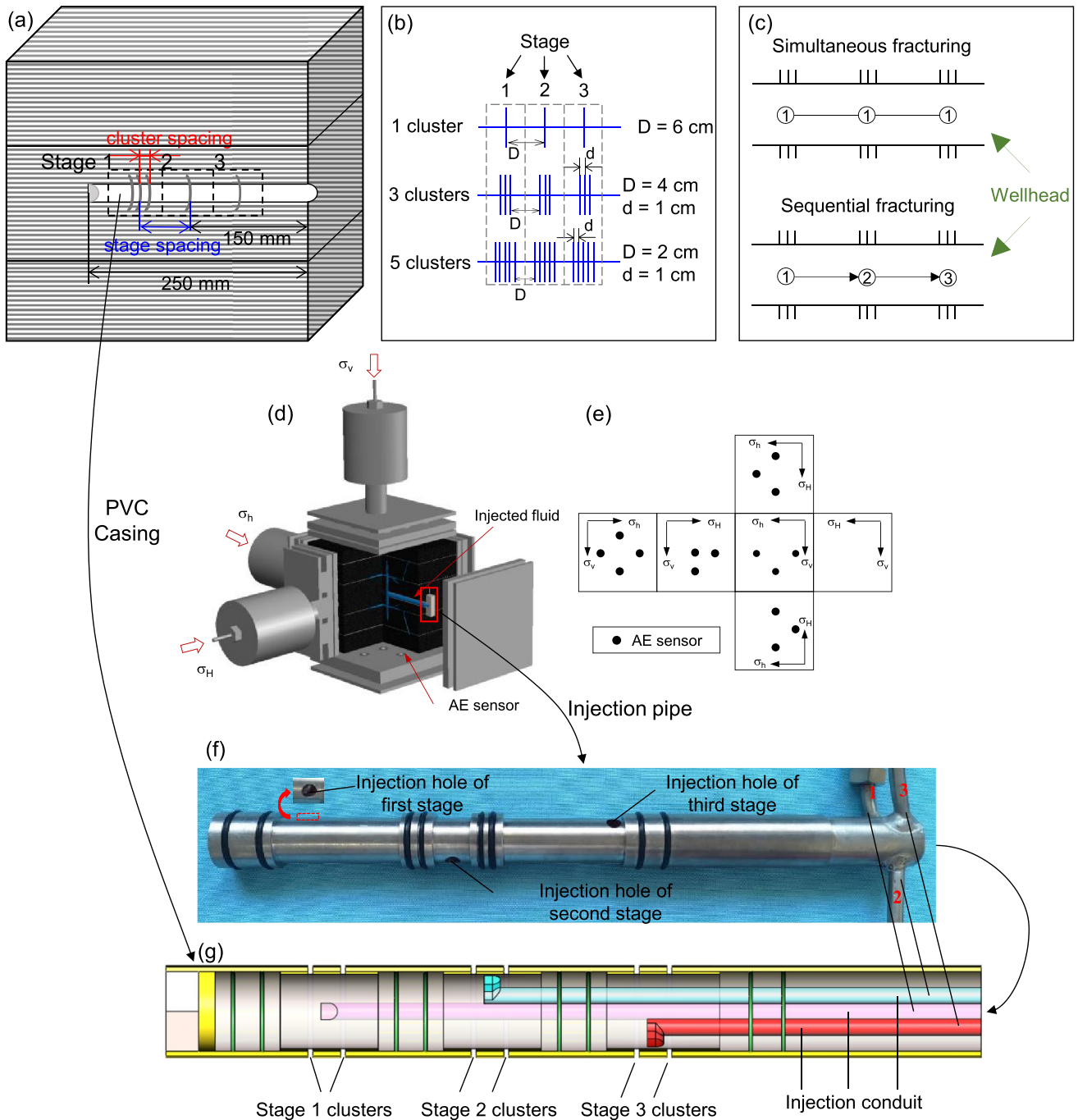


**Fig. 2** **a** Schematic diagrams of stage and cluster parameters. **b** Length of stage spacing and cluster spacing. **c** Schematic of simultaneous fracturing and sequential fracturing set in our experiment. **d** Tri-axial hydraulic fracturing experimental system with AE monitoring.

**e** Distribution of AE sensors. **f** Structure of the injection pipe inserted into the PVC casing. **g** Assembly diagram of the PVC casing and the injection pipe (modified from Zhang et al. 2021a)

to the bedding interface) on the sample is denoted as  $\sigma_v$  and the other two horizontal boundary loadings are respectively denoted as  $\sigma_H$  and  $\sigma_h$  (Fig. 2d). We use the same stress state (i.e.,  $\sigma_h = 10$  MPa,  $\sigma_H = 22$  MPa,  $\sigma_v = 30$  MPa) for all samples according to the in-situ stress state of the Lucaogou formation (Zhang et al. 2021a). To inject fluid in each stage, an

injection pipe with three injection conduits is assembled into a PVC casing, analogous to wellbore in the field (Fig. 2f, g). The samples are carefully prepared to guarantee that the PVC casing is well coupled with the rock matrix, and no water can spill along the bonding surface.

The DS5 multi-channel continuous waveform AE system is used for AE waveform acquisition. A total of sixteen RS-2A AE sensors with stable frequency response at 50–400 kHz are arranged on the five surfaces (i.e., top, left, right, front, and back) of the rock sample (Fig. 2e). According to the hypothesis of the far-field source, the inversion of the AE source at an appropriate position needs to be more than two wavelengths away from the sensors. All the sensor positions in the samples are in this acceptable area. The amplitude threshold of each sensor is set to 100 mV, and the preamplifier is 40 dB. The continuous waveform acquisition mode is adopted, and the sampling rate is set to 3 MHz per sensor. The pencil lead-breaking calibration in terms of amplitude has been conducted, which provides data for verifying AE event location and moment tensor inversion. We calibrate the sensor and algorithm following the method of Ono (2016) and Grosse and Ohtsu (2008). The calculation of AE event location is based on the classical Geige method. Since shale is composited of layered depositions, we use the transversely isotropic model to describe the *P*-wave anisotropy to achieve more accurate results. The arrival times and the amplitudes are determined from the AE waveforms by the STA/LTA–AIC picker method (Sedlak et al. 2013; Zhang et al. 2017).

The fracture properties are distinguished by the polarity of the first arrival of *P*-wave, which has been used in many previous works (Lei et al. 2000, 1992; Li et al. 2018b; Ma et al. 2017; Meglis et al. 1995; Satoh et al. 1990). Two polarity types of *P*-wave first motions may be detected. The downward polarity (after calibration) of the first motions of *P*-wave represents the negative type of waveform, while the upward polarity indicates a positive type. The negative and positive types of waveforms are determined by the deformation of the medium around the fractures caused by their movement. When a fracture opens or slips, the involved medium area is compressed, and the others are dilatated relative to the hypocenter position. The dilatation part will show a negative type of waveform, while the compression part presents a positive type. The proportion of the number of positive type waveforms is used as a criterion to determine the type of the corresponding AE event. Specifically, if the proportion of the number of positive type waveforms is larger than 0.7, a large area around the fracture is subjected to compression, and thus the fracture can be deemed as tensile type; if the proportion is somewhere between 0.3 and 0.7, the fracture is of shear-type; if the proportion is smaller than 0.3, the fracture is likely of compressive-type. Particularly, the compressive AE events are “collapse” mechanism sources containing a predominant collapse component, and they require shearing between grains to be physically achievable for new fractures. Such processes may relate to the collapse of existing fractures, pore spaces, and crushing of grains at high confining pressures. Graham et al. (2010)

discussed that this type of failure may be a part of those events with an implosive volume deformation and could be further studied by the moment tensor technique in more detail. Based on the statistics of *P*-wave polarity, each AE event can be categorized into tensile, shear, or compressive types.

### 2.3 Injection Design

To shed light on the field scale engineering application, the injection parameters in laboratory experiments must be designed based on the scaling laws connecting experiments with the field results. According to the scaling law, the stage spacing and cluster spacing in laboratory experiments can be scaled to these in the field by (Zhang et al. 2021b):

$$\frac{S_M}{S_F} = \frac{L_M}{L_F}, \quad (2)$$

where the subscript M and F represent the parameters in the experiment and the field, respectively;  $S_M$  and  $L_M$  are respectively the cluster (or stage) spacing and the half-length of a fracture in the experiment, and  $S_F$  and  $L_F$  are those in the field. Here,  $L_M$  is ~0.15 m, and  $L_F$  is ~200 m. Therefore, the stage spacing  $D=6$  cm corresponds to  $S_F=80$  m,  $D=4$  cm corresponds to  $S_F=66$  m,  $D=2$  cm corresponds to  $S_F=33$  m, and the cluster spacing  $d=1$  cm corresponds to  $S_F=13$  m (Fig. 2b).

We select the injection rate based on previous experiments where the injection rate for shale is chosen from 5 to 100 ml/min (Li et al. 2020; Liu et al. 2020b; Zhang et al. 2021a, b). Results show that a higher injection rate could reduce the influence of fluid leak-off and increase the pressure build-up rate, which facilitates the penetration of hydraulic fractures through the bedding structures. Recent research even uses an injection rate of 500 ml/min to investigate the effect of bedding interfaces on hydraulic fracturing and suggests that a higher injection rate may promote the propagation of fractures in shale oil reservoirs (Huang and Liu 2017). By considering the penetration of bedding structures, we choose a 300 ml/min injection rate in our current experiments, and also set a 100 ml/min injection rate for comparison.

Two modes of fracturing procedure have been conducted in our experiment, i.e., simultaneous fracturing and sequential fracturing (Fig. 2c). In simultaneous fracturing, the fluid is injected at the three stages simultaneously (top panel of Fig. 2c). After the simultaneous fracturing, we also inject the fluid at each stage individually to check the fracturing effect (i.e., checking injection). The injection rate of the checking injection is the same as the previous injection in each sample. Therefore, we should observe four sections on the injection pressure curve for the simultaneous fracturing experiment (as

will be shown in Fig. 3a–d). If a high injection pressure and a new fracture initiation are observed in the checking injection, it is highly likely that the specific stage is not stimulated during the simultaneous fracturing. If the checking injection witnesses a flat injection pressure, it means the specific stage is either stimulated or linked up with other stages during the simultaneous fracturing. The simultaneous fracturing mode could be used to investigate the simultaneous propagation of multiple fractures in the shale oil rocks.

In sequential fracturing, we inject the fluid stage by stage (bottom panel of Fig. 2c, from Stage 1 to Stage 3), and thus three sections could be observed on the injection curves (as will be shown in Fig. 3e–f). It is worth noting that in the field hydraulic fractures could hold the net pressure during the sequential fracturing; however, because of the fast backflow of fluid into the pipelines and fluid filtration in the boundary in laboratory experiments, the net pressure dropped quickly when ceasing the injection. The fractures without continuous net pressure are easily closed and cause little stress shadow on the subsequent fractures, which is not consistent with the situation in the field but could be used to investigate the propagation of fractures without the effect of stress shadow. The results could clarify the influence of lamination and bedding interface on the hydraulic fractures during the propagation of multiple fractures without disturbance from stress shadow.

Based on the above experimental setup and parameter selection analysis, we have chosen six samples that vary in

cluster number, injection rate, bedding interface, and fracturing mode under the in-situ stress of Lucaogou formation for current laboratory experiments. The corresponding parameters for the six samples are demonstrated in Fig. 4. Specifically, the Sample 1 and Sample 2 (with 1 and 3 clusters per stage, respectively; without bedding interface adhesion; 300 ml/min injection rate; simultaneous fracturing) are selected to compare the stimulation effect of different number of clusters; the Sample 1 and Sample 3 (with 1 cluster per stage; without bedding interface adhesion; 300 and 100 ml/min injection rate, respectively; simultaneous fracturing) are employed to investigate the effect of injection rate; the Sample 3 and Sample 4 (with 1 cluster per stage; without and with bedding interface adhesion, respectively; 100 ml/min injection rate; simultaneous fracturing) are conducted to investigate the influence of bedding interface; the Sample 5 (with 1 cluster per stage; with bedding interface adhesion; 300 ml/min injection rate; sequential fracturing) is prepared to clarify the impact of lamination and bedding interface on the multiple fractures propagation without disturbance from stress shadow; the Sample 6 (with 5 cluster per stage, with bedding interface adhesion; 300 ml/min injection rate; sequential fracturing) is selected as a supplement to ensure a successful propagation of multiple fractures under the laboratory condition. The influence of cluster number per stage, injection rate, bedding interface, and fracturing mode are analyzed and presented in the next section.

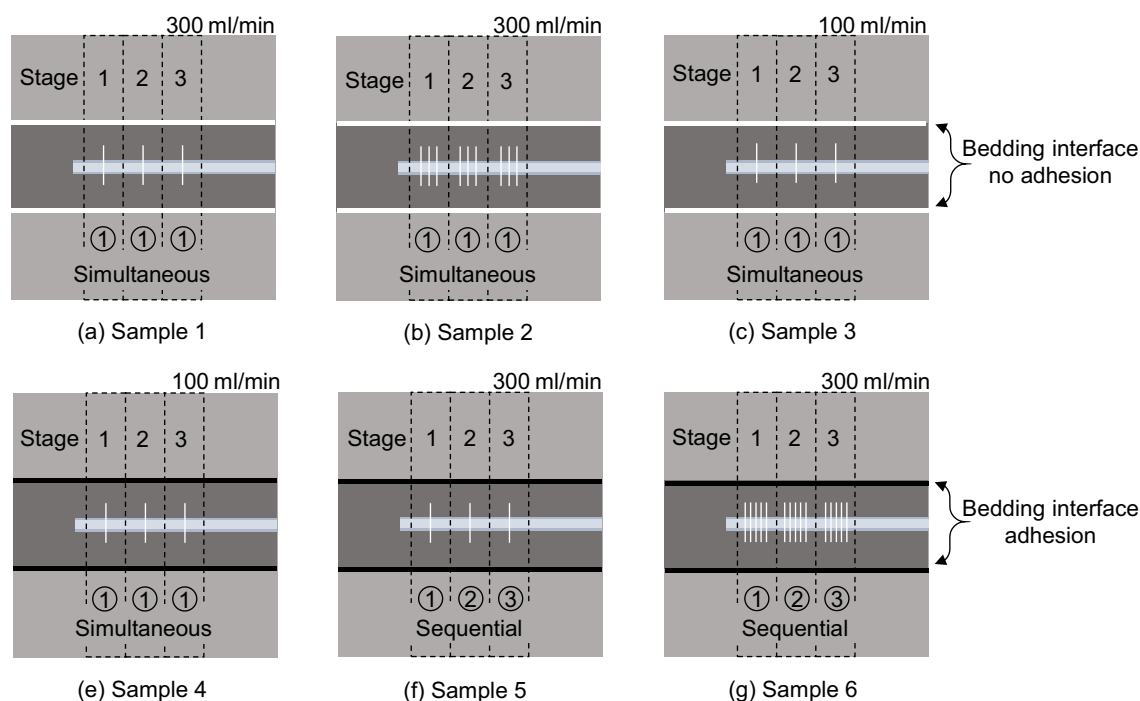


**Fig. 3** Schematic diagrams of the six samples used in the current laboratory experiments

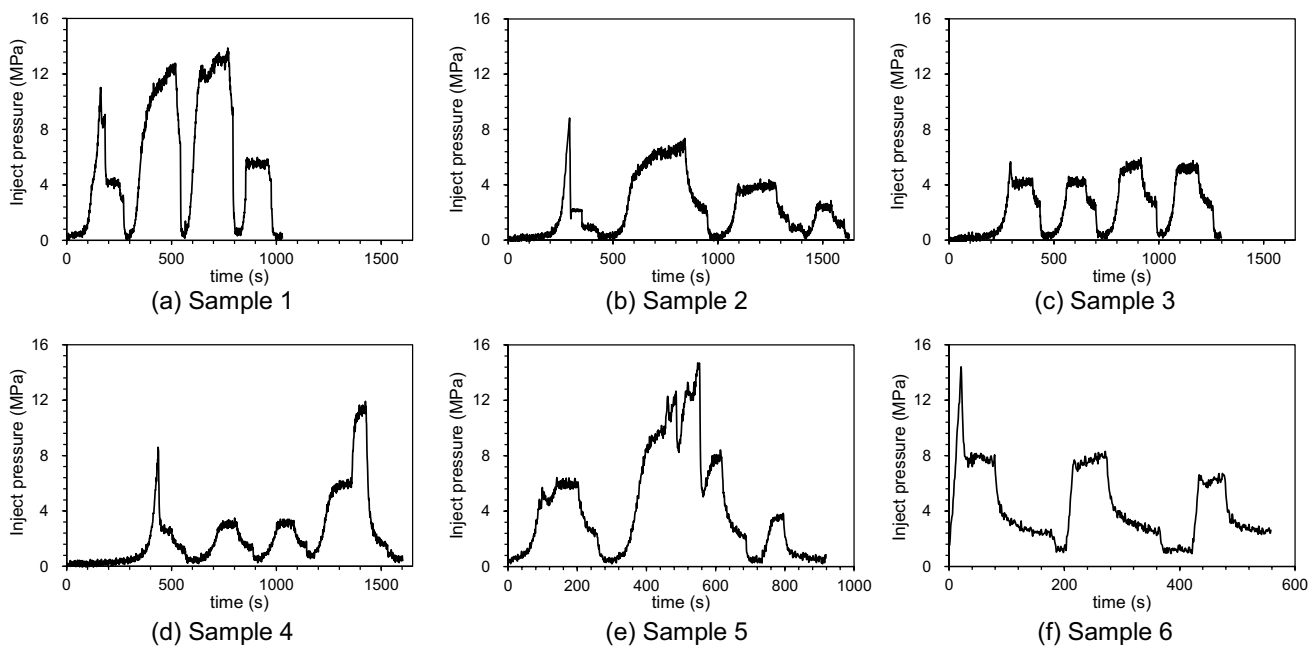


Fig. 4 Injection pressure curves of the six samples

### 3 Results

In this section, to investigate the impact of different factors on multiple fractures fracturing, we use the AE locations to show the propagation of multiple fractures in each sample. Then, the shear–tensile properties of fractures distinguished

by AE events are applied to reveal the mechanism of fracture interference among multiple fractures, and the injection pressure of each sample is utilized to deduce whether the lamination and bedding interface could induce the filtration of fracturing fluid.

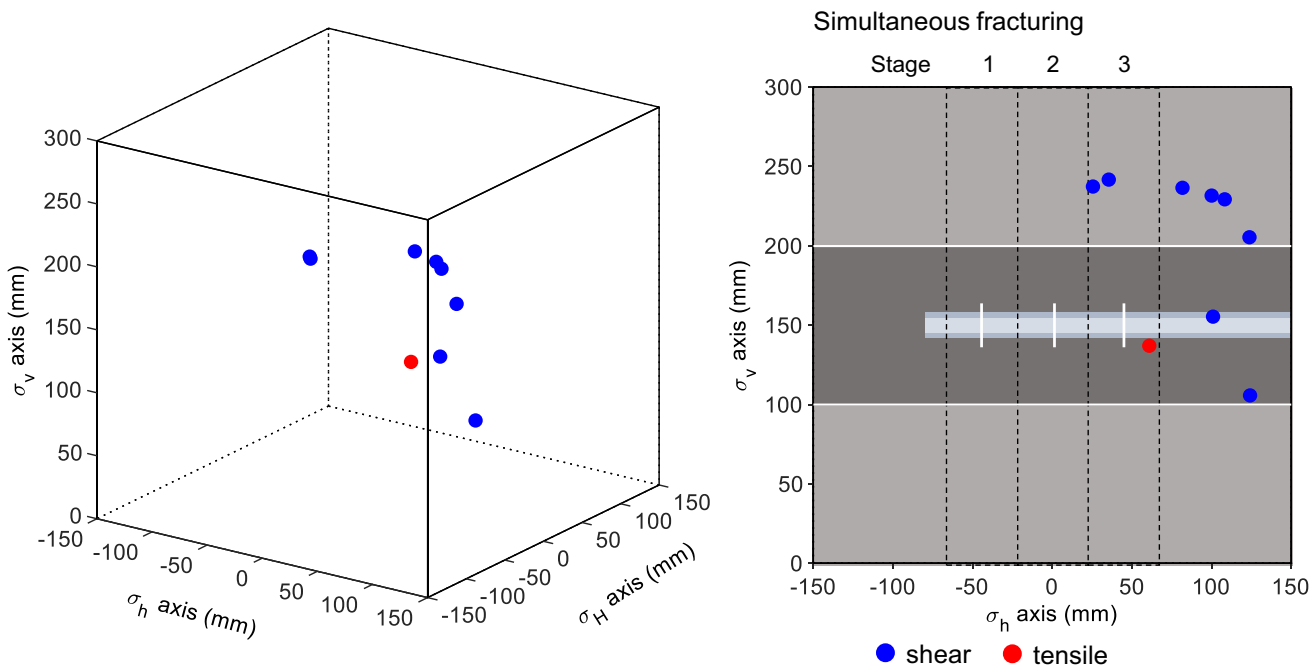


Fig. 5 AE event location result of Sample 1. There are nine AE events: eight shear-type (blue), and one tensile-type (red)

### 3.1 Influence of Cluster Number and Injection Rate

Sample 1 and Sample 2 are used to investigate the influence of the number of clusters per stage on the propagation of multiple fractures, and both of them are fabricated without bedding interface adhesion. Sample 1 is cut with one cluster per stage, and the simultaneous fracturing mode with a high injection rate of 300 ml/min is performed on it (Fig. 4a). The AE location interpretation shows a few AE events in the area of Stage 3 (Fig. 5). One tensile-type AE event appears near the wellbore, and several shear-type AE events distribute at a distance away from the wellbore. The AE results show a small number of fractures initiated near the area of Stage 3. The hydraulic fractures barely expand, and the filtration of fracturing fluid along the bedding interface has been observed. The injection pressure during the simultaneous fracturing peaks at 11.0 MPa (the first peak in Fig. 3a) and drops quickly to ~4.0 MPa. The checking injection pressure shows a stable value of 12.0 MPa in the first checking injection (in Stage 1), 13.0 MPa in the second (in Stage 2), and 5.1 MPa in the third (in Stage 3) (the last three peaks in Fig. 3a), indicating that no new hydraulic fractures have been induced. The third checking injection pressure in Stage 3 is lower than that in Stage 1 and 2, but higher than the stable pressure after dropping from the peak pressure in the simultaneous fracturing. Combined with the AE results, we infer that the fractures in the area of Stage 3 propagate a little bit (indicated by the tensile-type AE events) but are

filtered out of the boundary from the bedding interface (indicated by the shear-type AE events near the bedding interface). There is no clear fracture propagation in Stage 1 and 2 (i.e., no AE events), and the fluid may slip out of the boundary along the lamination. Because the permeability of the lamination is lower than that of the bedding interface, the flow resistance in Stage 1 and 2 are higher than that in Stage 3. Therefore, the checking injection pressures in Stage 1 and 2 are higher than the pressure in Stage 3.

Sample 2 has three clusters per stage, and it is also conducted under the simultaneous fracturing mode with the same injection rate of 300 ml/min as Sample 1 (Fig. 4b). The AE event locations in Sample 2 show that the fractures appear at all three stages (Fig. 6). Most of the tensile fractures are concentrated in areas between Stage 1 and 2, while the AE events in Stage 3 are mainly of shear-type. More AE events in Sample 2 than that in Sample 1 indicate that more clusters could promote the initiation of hydraulic fractures to a certain extent. However, the propagation of multiple fractures is still insufficient because the AE events are almost near the wellbore. The injection pressure during the simultaneous fracturing reaches a peak value of ~8.8 MPa, while the pressures in the process of checking injection hold up to 6.4 MPa for Stage 1, 3.9 MPa for Stage 2, and 2.6 MPa for Stage 3 (Fig. 3b). We infer that the fractures in Stage 1 terminate near the wellbore due to fluid filtration in the lamination, and the fractures in Stage 2 connect the fractures

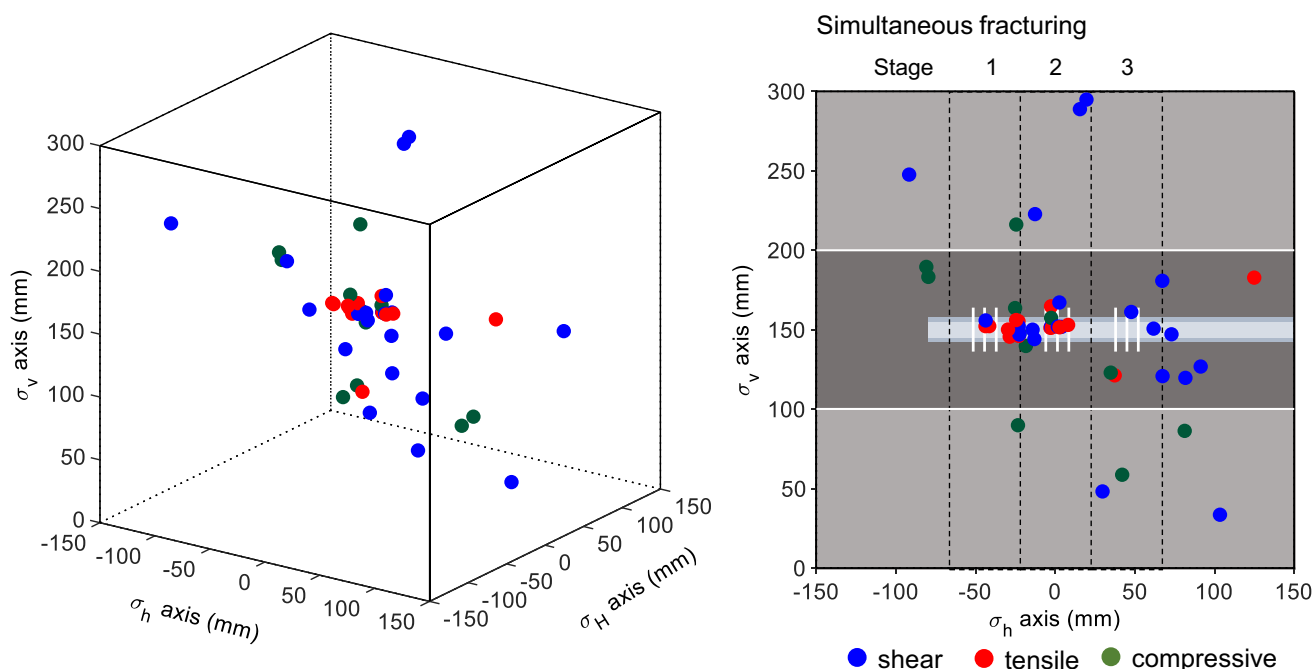


**Fig. 6** AE event location result of Sample 2. There are 48 AE events: 22 shear-type (blue), 14 tensile-type (red), and 12 compressive-type (green)

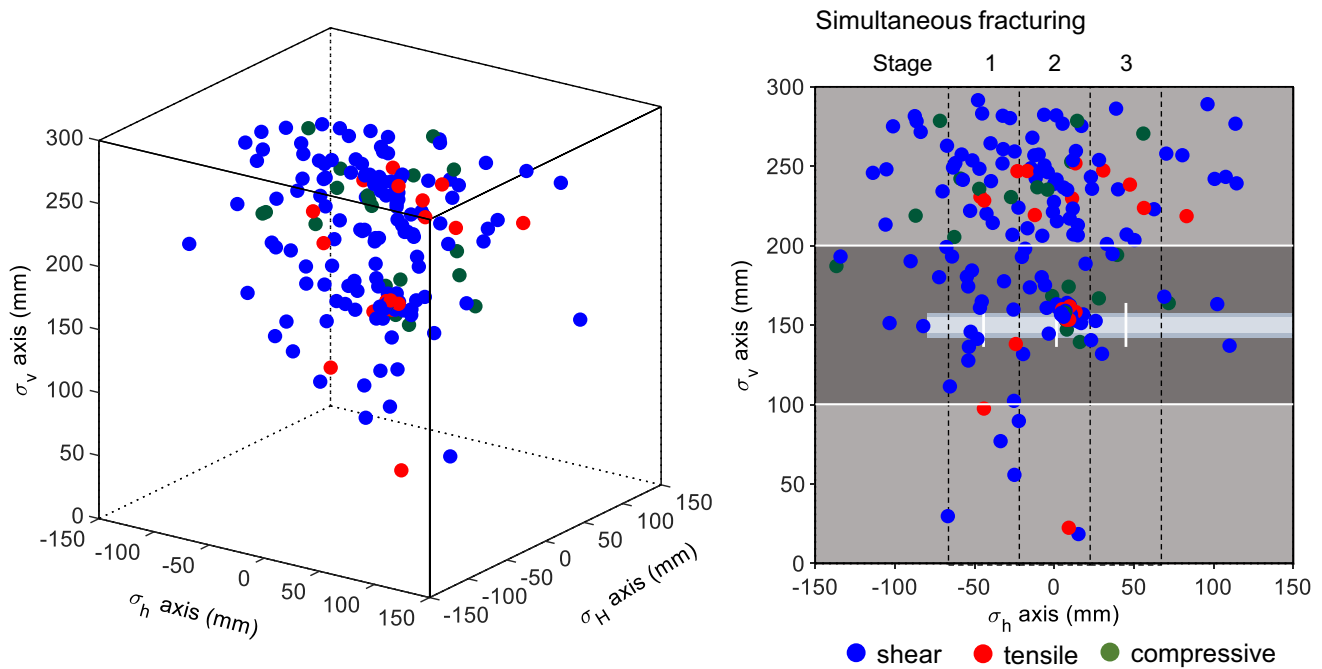


**Fig. 7** AE event location result of Sample 3. There are 178 AE events: 135 shear-type (blue), 20 tensile-type (red), and 23 compressive-type (green)

in both Stage 1 and 2 in areas near the wellbore, while the fractures in Stage 3 link the bedding interface.

The injection rate of fluid influences simultaneous fracturing because it controls the pressure distribution of the fracturing fluid in the wellbore. We reduce the injection rate in the experiment of Sample 3 (with one cluster per stage, but without bedding interface adhesion) to 100 ml/min and perform the simultaneous fracturing mode (Fig. 4c). From the results of AE events shown in Fig. 7, it is found that there are more AE events in the areas of Stage 1 and Stage 2, and they are mainly of shear-type. This indicates that the fluid promotes the shear-type fractures inside the rock, which may be caused by the activation of lamination that leads to slipping inside the rock. The AE events are mainly distributed in the upper layer of the rock, and nearly no AE events occurred in the lower layer. A few tensile-type AE events appear in the upper layer, meaning some tensile fractures propagate in the upper part. This is possible due to the penetration of hydraulic fractures through the bedding interface locally under the given  $\sigma_v$  pressure. The little propagation of fractures in the lower layer may be caused by the filtration of fluid in the non-adhesive bedding interface. The injection pressure during the simultaneous fracturing reaches a maximum value of 5.7 MPa, lower than the values in Sample 1 and Sample 2 (Fig. 3c). The pressures in each stage in the checking injection process are nearly the same at around 5 MPa.

The above results demonstrate that in the simultaneous fracturing mode, more AE events are obtained when a lower injection rate is used, and the primary type of AE events is shear. We suspect that reducing the flow rate makes the fluid pressure more evenly distributed in the wellbore, which is beneficial to fracture initiation in the Lucaogou formation. However, because there are laminations and bedding interfaces in this rock formation, it is easy for fracturing fluid to be filtered in the laminations and bedding interfaces when using low injection rates. According to the results of Samples 1, 2, and 3, although increasing the number of clusters per stage and reducing the injection rates could facilitate the initiation of fractures, it is challenging to promote the propagation of fractures in simultaneous fracturing mode in the Lucaogou formation.

### 3.2 Impact of Bedding Interface

Sample 4 has adhesive beddings and is subjected to simultaneous fracturing, and its comparison with Sample 3 (without bedding interface) could reveal the influence of bedding interface. In Sample 4, the propagation of multiple fractures mainly occurs in the areas of Stage 1 and 2, but the fractures in the Stage 3 area are constrained in the direction of  $\sigma_v$  (Fig. 8). Compared with the non-adhesion Sample 3 under the same injection condition (same injection rate and fracturing mode), the propagation of multiple fractures in Sample 4 is abundant, as indicated by a large number of generated AE

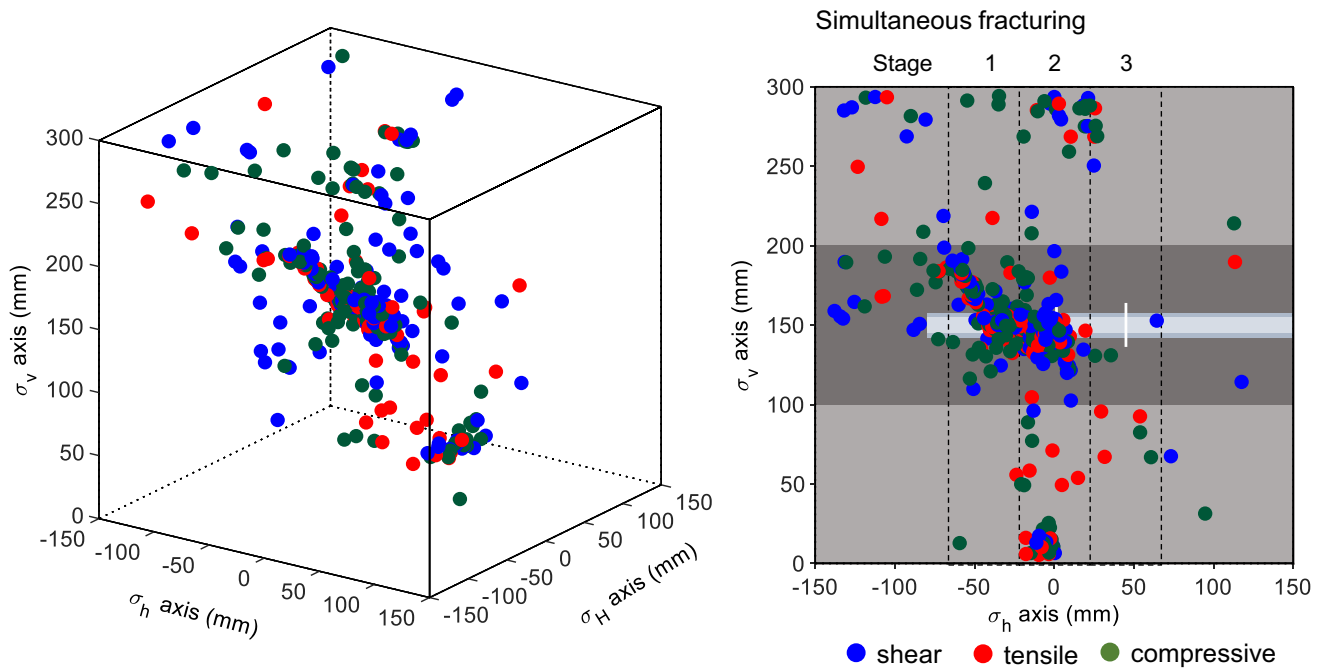


**Fig. 8** AE event location result of Sample 4. There are 523 AE events: 178 shear-type (blue), 120 tensile-type (red), and 225 compressive-type (green)

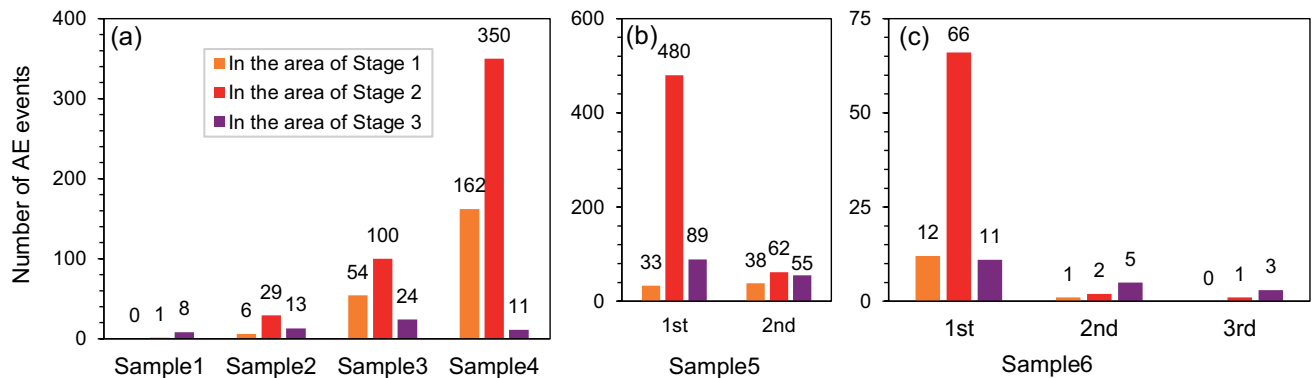


**Fig. 9** Number of AE events in different stages for each sample

events (Fig. 9a). The injection pressure during the simultaneous fracturing reaches 8.6 MPa, while the checking injection pressures in Stage 1 and Stage 2 are both 3.0 MPa and that in Stage 3 is stabilized at 5.7 MPa (Fig. 3d). The injection pressures are consistent with the distribution of AE events such that the AE events in the areas of Stages 1 and 2 are almost linked together, while the AE events barely occur in the area of Stage 3. We suspect that the fluid in Stage 1 and 2 is linked through the lamination and bedding interface, while the fluid in Stage 3 is isolated.

The propagation of multiple fractures in the area of Stage 2 is vertically symmetrical, and many of them are of

tensile-type. During the propagation, uneven fracture growth is typical due to fracture interference, and the distribution of AE events confirms this. We use the following equation to calculate the asymmetry distribution of AE events:

$$A = \frac{|n_1 - n_2|}{N}, \quad (3)$$

where  $n_1$  and  $n_2$  are the numbers of AE events on the two sides of the symmetry plane, and  $N$  is the total number of AE events. If the fractures are symmetrical, the ratio would be 0; if all the AE events occur on one side, the ratio is 1. Since Sample 1 has only 8 AE events, it is not meaningful to

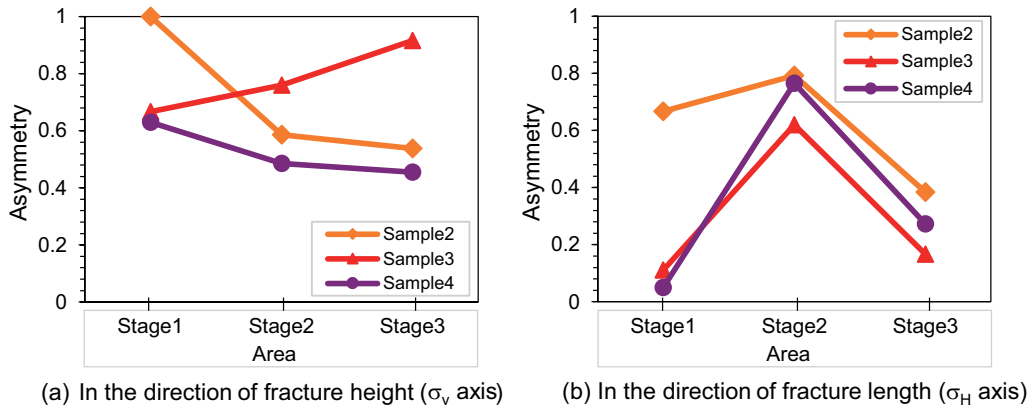


**Fig. 10** Asymmetry ratios of multiple fractures for each sample in various stages

calculate the asymmetry ratio. We calculate the asymmetry distribution of AE events for Samples 2 to 4. In the direction of fracture height (i.e., the direction of  $\sigma_v$ ) (Fig. 10), Sample 4 has a lower asymmetry ratio than Sample 2 and Sample 3 in all stages. This may be because the adhesive bedding interface has a balancing effect on the distribution of fracturing fluid. While in the samples without adhesive bedding interfaces (Samples 2 and 3), the fluid may filter out of the bedding interface on one side, resulting in the unbalance of fluid distribution. The asymmetry of fractures in the direction of fracture length (i.e., the direction of  $\sigma_H$ ) demonstrates that the fractures in the area of Stage 2 show higher asymmetry for all samples. This is consistent with the previous research that the interior fractures generally show uneven growth due to the additional compressional stress from both sides of the exterior fractures (Wu and Olson 2016; Zhang et al. 2021b).

Theoretically, the fractures should distribute symmetrically in the direction of fracture length if the rock is homogeneous or lateral heterogeneous. However, shales are barely homogeneous even on the lateral plane. Many numerical studies indicated that the heterogeneity of rock could induce asymmetrical fractures. Wu et al. (2022) found that the heterogeneity of Young's modulus would lead to asymmetric propagation of a single fracture. For multiple fractures, the results from 3D simulation also indicated asymmetric fractures under the influence of heterogeneous Young's modulus (Ren et al. 2019). Yang et al. (2020) made further investigation and showed that besides Young's modulus, the heterogeneity in tensile strength and permeability could also induce the asymmetry of fractures. Therefore, it is unavoidable that in our experiments the asymmetric fractures could be easily observed. In addition, the bedding structures could also violate the fracture propagation by disturbing the net pressure, which may be another reason for the generation of asymmetric fractures.

### 3.3 Effect of Fracturing Mode

We perform the sequential fracturing mode with an injection rate of 300 ml/min for Sample 5 with bedding interface adhesion to investigate the influence of lamination and bedding interface on multiple fractures propagation without disturbance from stress shadow. For the first injection, although the fluid is injected in Stage 1, the fractures are mainly concentrated around the upper half area of Stage 2 and the lower half area of Stage 3, as is manifested by the AE location shown in Fig. 11a. This may be related to the transformation of fluid through laminations. The injection pressure reaches a first peak value of around 5.7 MPa and stabilizes at 6.4 MPa (Fig. 3e). The appearance of the first pressure peak may be due to the opening of fractures near the wellbore. Then the hydraulic fractures are captured by the bedding interface, and result in a stable injection pressure. In the second injection (injected in Stage 2), there are many shear-type AE events appeared near the area of Stage 2, and the injection pressure is higher than that of the first injection (Fig. 3e). The numerous shear-type AE events in the mid-layer of the rock and the associated higher injection pressure indicate that the fluid is filtered through the lamination during the second injection. The tensile-type AE events that occurred in the area of Stage 3 signal that the filtered fluid from Stage 2 causes the opening of fractures in the area of Stage 3 (Fig. 11b). However, we barely obtain AE events in the third injection (injected in Stage 3) and the injection pressure during this process is relatively small (Fig. 3e). By combining the above experimental results, we deduce that the propagation of fractures in Stage 1 could affect that in Stage 2. The extending range of hydraulic fractures in the second injection is short, and there are no fractures in the third injection. Because there is no net pressure in the previous fractures during the sequential fracturing, the impact of the already generated fractures on the new fractures lies

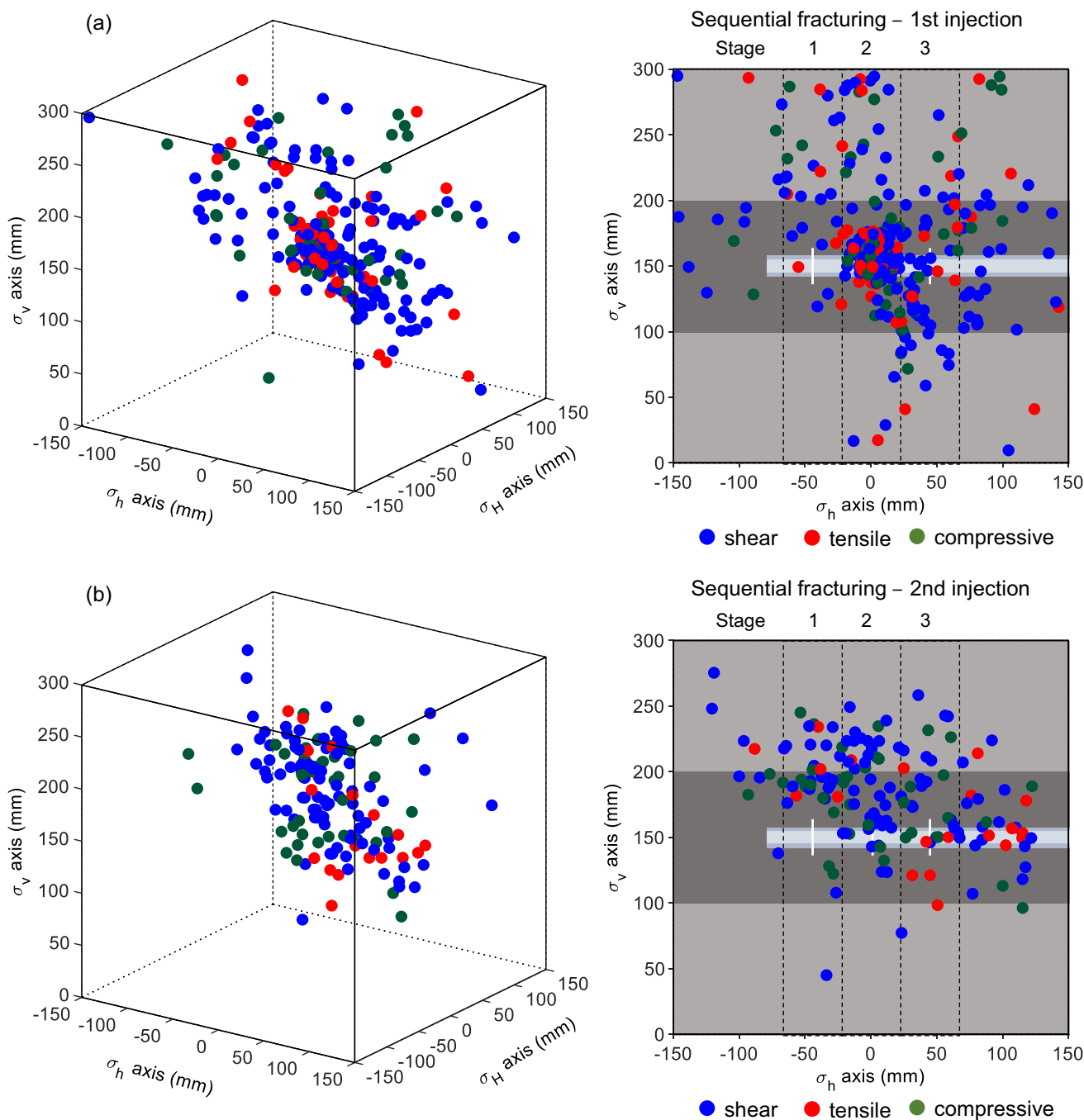


**Fig. 11** **a** AE event location in Sample 5 in the first injection; a total of 602 AE events have been acquired: 350 shear-type (blue), 123 tensile-type (red), and 129 compressive-type (green). **b** AE event loca-

tion in Sample 5 in the second injection; a total of 155 AE events have been collected: 95 shear-type (blue), 20 tensile-type (red), and 40 compressive-type (green)

in the laminations and bedding interfaces being penetrated by the former.

The sequential fracturing mode is also conducted for Sample 6 with bedding interface adhesion, with 5 clusters per stage and an injection rate of 300 ml/min. The AE event location of the first injection (injected in Stage 1) is shown in Fig. 12a. In the area of Stage 1, we can observe tensile

fractures distributed near the wellbore, with a few shear fractures occurring at a distance away from the wellbore. Although injected at Stage 1, many tensile fractures appear in the area of Stage 2, and these fractures propagate through the upper and lower bedding interfaces, indicating that the fluid from Stage 1 completely transfers to Stage 2 near the wellhead and causes the propagation of fractures in the area

of Stage 2. Then in the second injection (injected in Stage 2), there are no tensile-type AE events (Fig. 12b), which indicates that Stage 2 has been fractured in the first injection. There are few AE events in the third injection (injected in Stage 3) (Fig. 12c). Compared with all other samples, the pressure in this first injection in Sample 6 is the highest—14.4 MPa (Fig. 3f), which indicates that the multiple fractures are stimulated sufficiently with less fluid filtration. The injection pressures in the second and third injections are stabilized at 7.5 MPa and 6.4 MPa respectively, which reflects the filtration of fluid in these two injections due to the influence of the first injection.

For the above two samples (Sample 5 and Sample 6) subjected to the sequential fracturing mode, the AE events mainly occur in the first injection and most of them are of shear type, with a few appearing in the second and third injection (Fig. 9b, c). During the second injection, there are more shear-type AE events generated. The influence of the first injection on the second may be transmitted not only by “stress shadow” but also by the activation of bedding interface. In the case with 5 clusters (Sample 6) where the stage spacing is smaller than all other samples, in the first injection, more tensile fractures are induced in the area around Stage 2, and the fractures extend to the model boundary. In the second and third injections, there is almost no AE event. This reveals that when the cluster spacing is small, the fracture interference even occurs during the initial process of hydraulic fracturing. Such fracture interference in the initial hydraulic fracturing process due to the opening of bedding interface has also been observed elsewhere in the Longmaxi Shale (Zhang et al. 2021b), although with the fact that this is more likely to appear in the Lucaogou formation with lamination and bedding interface.

## 4 Discussions

### 4.1 Shear-Type AE Events and the Activation of Lamination and Bedding Interface

In general, tensile-type fractures are dominant in hydraulic fracturing under the stimulation of high-pressure fluid. However, a large amount of shear-type AE events have been obtained in our experiments, especially in processes under the following conditions: (1) when the initiation of fracturing is difficult (Sample 1); (2) when asymmetric fractures appear (Sample 4); (3) when obvious fracture interferences occurred (the second injection of Sample 5, second and third injections of Sample 6) (Fig. 13). The laminations and bedding interface play a key role in such results. Specifically, first, the existence of laminations and bedding interface leads to the heterogeneity of local stress, making the direction of fracture propagation deviate from the maximum

far-field principal stress direction, and this results in a more significant shear action on the surface of hydraulic fractures; second, the laminations and bedding interface have a particular filtration effect on the fracturing fluid, and thus when interacting with fluid, the laminations and bedding interface could increase local dislocation and friction and result in shear fractures.

### 4.2 Fracture Interference in Reservoirs with Lamination and Bedding Interface

For simultaneous multiple fracture propagation in a single stage, the influence of fracture interference on the propagation of fractures is a significant problem in reservoirs. Stress shadow is one of the causes of fracture interference, according to the previous research for reservoirs without lamination and bedding interface (Wu and Olson 2015, 2016). The stress shadow induced by a single hydraulic fracture can be obtained by

$$\sigma'_x = p \frac{r}{c} \left( \frac{c^2}{r_1 r_2} \right)^{\frac{3}{2}} \sin \theta \sin \frac{3}{2} (\theta_1 + \theta_2) + p \left[ \frac{r}{(r_1 r_2)^{\frac{1}{2}}} \cos \left( \theta - \frac{1}{2} \theta_1 - \frac{1}{2} \theta_2 \right) - 1 \right] \quad (4)$$

and

$$\sigma'_y = -p \frac{r}{c} \left( \frac{c^2}{r_1 r_2} \right)^{\frac{3}{2}} \sin \theta \sin \frac{3}{2} (\theta_1 + \theta_2) + p \left[ \frac{r}{(r_1 r_2)^{\frac{1}{2}}} \cos \left( \theta - \frac{1}{2} \theta_1 - \frac{1}{2} \theta_2 \right) - 1 \right], \quad (5)$$

where  $c$  is the half of the fracture height,  $p$  is the net pressure in the hydraulic fracture, and  $r$ ,  $r_1$ ,  $r_2$ ,  $\theta$ ,  $\theta_1$ ,  $\theta_2$  are geometrical parameters explained in Fig. 14. The above formulas work when the width of the elliptical fracture is much smaller than its length, which is suitable for hydraulic fractures. Equations (4) and (5) indicate that the amplitude of stress shadow depends on the amplitude of net pressure of the hydraulic fracture, which is consistent with other research (Manchanda et al. 2017; Taghichian et al. 2014). However, the net pressure could not be directly measured in the experiment. The lamination and bedding interfaces may influence the net pressure and change the stress shadow and thus cause fracture interference.

In addition to the net pressure, the hydraulic fluid flowing into the lamination and bedding interface may increase the pore pressure, which then induces more fractures of shear-type than tensile-type. In addition, the higher pore pressure may trigger the slip of bedding interface, which also leads to more shear-type AE events during the propagation of

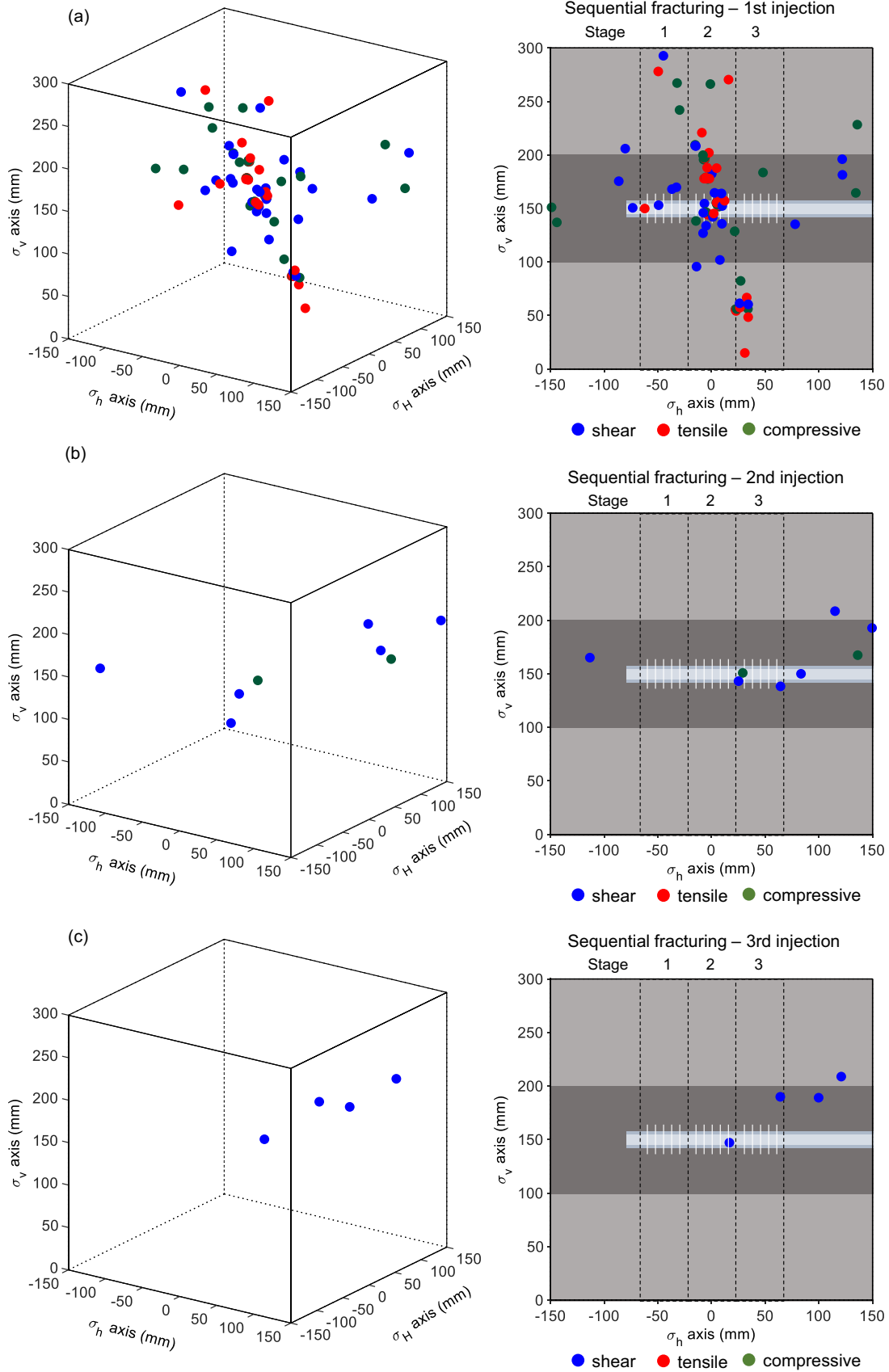


**Fig. 12** **a** AE event location result of Sample 6 in the first injection; a total of 89 AE events have been acquired: 28 shear-type (blue), 30 tensile-type (red), and 31 compressive-type (green). **b** AE event location result of Sample 6 in the second injection; a total of 8 AE events have been acquired: 6 shear-type (blue), 2 compressive-type (green), and no tensile-type (red). **c** AE event location result of Sample 6 in the third injection; a total of 4 shear-type (blue) AE events have been acquired

hydraulic fracture. The appearance of sufficient shear-type fractures signifies the fracture interference in the reservoir. The fracture interference is even more severe in reservoirs with lamination and bedding interfaces. Moreover, we note that the hydraulic fluid is easy to flow out of the boundary of the rock sample containing structures with high permeability in the experiment. The loss of fluid reduces the net pressure and thus could limit the direct applicability of laboratory experiments, since in real reservoirs without apparent boundaries there is generally less fluid loss. We take the results of AE events as a supplement to investigate the propagation of hydraulic fractures in the limited condition mentioned above and provide more evidence to study the mechanism of fracture interference. However, the loss of fluid cannot be avoided in laboratory experiments.

In addition, the fracture interference is more complicated, as evidenced by the irregular and asymmetric fracture propagation. Our results show significant asymmetry ratios in each fracture (Fig. 10) and in Stage 1 and 3. The lamination and bedding structures contribute to the heterogeneity of the sample, which leads to an asymmetrical stress state and mechanical properties of the rock matrix, thus result in the asymmetric propagation of fractures. In addition, Stages 1 and 3 are relatively close to the boundary of the sample. The fracturing fluid is more likely to flow out of the sample during the two stages, and then disturbs the symmetry condition. All these factors of asymmetry contribute to the intricate fracture interference.

Many research suggests that widening the space of cluster and stage can reduce the stress shadow effect and avoid fracture interference (Wang et al. 2021). However, in the reservoir with lamination and bedding interfaces, the stress shadow around the hydraulic fractures is not the only reason for fracture interference. The change of pore pressure caused by the high permeability channel of the lamination, bedding interface, and heterogeneity could also significantly influence the propagation of multi-cluster fractures. Therefore,

it is necessary to evaluate the size and distribution of high permeability areas to avoid or alleviate fracture interference. Besides, the slip of bedding interface also causes a considerable disturbance of stress in the reservoir. Preventing the slip of bedding interface can help promote the effect of multi-cluster fracturing by avoiding the stress shadow effect.

## 5 Conclusions

In this paper, we use a true tri-axial hydraulic fracturing equipment combined with AE monitoring to study the multiple fracturing process in the Lucaogou shale. We consider the influence of cluster number, injection rates, fracturing mode, and the adhesion condition of bedding interface on the initiation and propagation of hydraulic fractures. Our experimental results show that even with a large stage and cluster space, the propagation of multiple fractures is still limited in the Lucaogou shale. Many shear-type AE events appear during the fracturing, which shows the influence of laminations and bedding interface on the propagation of hydraulic fracture. Even if the fluid pressure in the well is partitioned equally by reducing the injection rate, the influence of the lamination on the initiation and propagation of hydraulic fractures still exists. The adhesion situation affects the symmetry of fractures in the direction of fracture height. When the bedding is adhesive, the AE event distribution in the direction of fracture height is symmetrical; when the cementation of bedding interface is small, the AE event will concentrate on one side of the direction of fracture height. The asymmetric propagation of fractures makes the mechanism of fracture interference more complicated.

In the experiment of sequential fracturing, the fluid in the first stage communicates with other stages through the lamination and bedding interface near the wellhead. This leads to the shift of the position of fracture propagation in the initiation stage. With the existence of laminations and bedding interface, the influence of previous fractures on new cracks is from the stress shadow and the transfer of fluid pressure through the lamination and bedding interface. Therefore, for the multi-cluster and multi-stage fracturing in the Lucaogou formation, it is necessary to optimize the fracturing strategy considering the high permeability and heterogeneity of lamination and bedding interface.

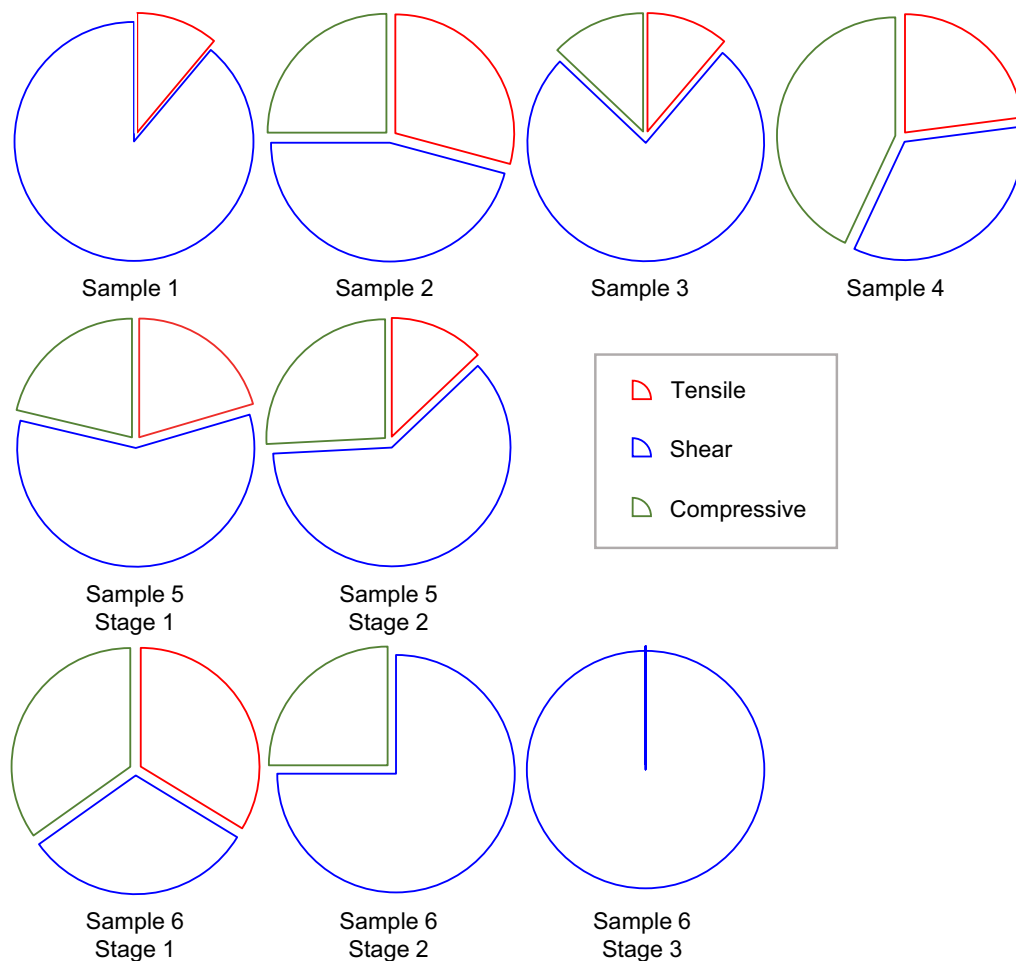


**Fig. 13** Proportions of the shear, tensile and compressive-type AE events for the six samples

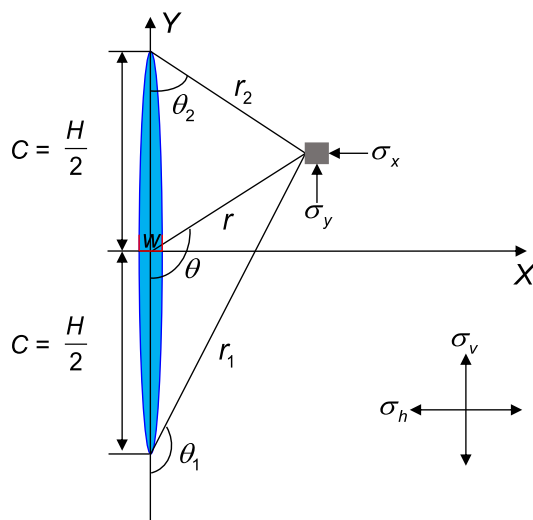


**Fig. 14** Stress distribution around the mode I type crack

**Acknowledgements** This work is financially supported by the sub-projects of the Strategic Cooperation Technology Projects of CNPC and CUPB (ZLZX2020-01-08 and ZLZX2020-01-07), and the Natural Science Foundation of China (no. 51774236).

## References

- Bunger A, Jeffrey RG, Zhang X (2014) Constraints on simultaneous growth of hydraulic fractures from multiple perforation clusters in horizontal wells. *SPE J* 19(04):608–620
- Crump J, Conway M (1988) Effects of perforation-entry friction on bottomhole treating analysis. *J Pet Technol* 40(08):1041–1048
- Graham CC, Stanchits S, Main IG, Dresen G (2010) Comparison of polarity and moment tensor inversion methods for source analysis of acoustic emission data. *Int J Rock Mech Min Sci* 47(1):161–169. <https://doi.org/10.1016/j.ijrmms.2009.05.002>
- Grosse CU, Ohtsu M (2008) *Acoustic emission testing*. Springer, Berlin
- Hampton JC, Hu D, Matzar L, Gutierrez M (2014) Cumulative volumetric deformation of a hydraulic fracture using acoustic emission and micro-CT imaging. In: 48th U.S. rock mechanics/geomechanics symposium, Minneapolis, Minnesota

- Hou B, Cheng W, Jin Y, Diao C, Zhang Y, Yang L (2014) Experimental investigation on fracture geometry in multi-stage fracturing under tri-axial stresses. In: ISRM international symposium-8th Asian rock mechanics symposium. international society for rock mechanics and rock engineering
- Huang B, Liu J (2017) Experimental investigation of the effect of bedding planes on hydraulic fracturing under true triaxial stress. *Rock Mech Rock Eng* 50(10):2627–2643. <https://doi.org/10.1007/s00603-017-1261-8>
- Huo J, He J, Gao Y, Dong Y, Xv D, Li Y (2019) Difficulties and countermeasures of shale oil development in lucaogou formation of Jimsar Sag. *Xinjiang Pet Geol* 40(4):379–388
- Ishida T, Labuz JF, Manthei G, Meredith PG, Nasserli M, Shin K, Yokoyama T, Zang A (2017) ISRM suggested method for laboratory acoustic emission monitoring. *Rock Mech Rock Eng* 50(3):665–674
- Lecampion B, Desroches J (2014) Simultaneous initiation of multiple transverse hydraulic fractures from a horizontal well. In: 48th US rock mechanics/geomechanics symposium. OnePetro
- Lei X, Kusunose K, Rao MVMS, Nishizawa O, Satoh T (2000) Quasi-static fault growth and cracking in homogeneous brittle rock under triaxial compression using acoustic emission monitoring. *J Geophys Res Solid Earth* 105(B3):6127–6139. <https://doi.org/10.1029/1999JB900385>
- Lei X, Nishizawa O, Kusunose K, Satoh T (1992) Fractal structure of the hypocenter distributions and focal mechanism solutions of acoustic emission in two granites of different grain sizes. *J Phys Earth* 40(6):617–634
- Li N, Zhang S, Zou Y, Ma X, Wu S, Zhang Y (2018a) Experimental analysis of hydraulic fracture growth and acoustic emission response in a layered formation. *Rock Mech Rock Eng* 51(4):1047–1062
- Li N, Zhang S, Zou Y, Ma X, Zhang Z, Li S, Chen M, Sun Y (2018b) Acoustic emission response of laboratory hydraulic fracturing in layered shale. *Rock Mech Rock Eng* 51(11):3395–3406
- Li S, Zhang S, Zou Y, Zhang X, Ma X, Wu S, Zhang Z, Sun Z, Liu C (2020) Experimental study on the feasibility of supercritical CO<sub>2</sub>-gel fracturing for stimulating shale oil reservoirs. *Eng Fract Mech* 238(May):107276–107276. <https://doi.org/10.1016/j.engfractmech.2020.107276>
- Liu N, Zhang Z, Zou Y, Ma X, Zhang Y (2018) Propagation law of hydraulic fractures during multi-staged horizontal well fracturing in a tight reservoir. *Pet Explor Dev* 45(6):1129–1138. [https://doi.org/10.1016/S1876-3804\(18\)30116-2](https://doi.org/10.1016/S1876-3804(18)30116-2)
- Liu X, Rasouli V, Guo T, Qu Z, Sun Y, Damjanac B (2020a) Numerical simulation of stress shadow in multiple cluster hydraulic fracturing in horizontal wells based on lattice modelling. *Eng Fract Mech* 238:107278. <https://doi.org/10.1016/j.engfracmech.2020.107278>
- Liu Z, Ren X, Lin X, Lian H, Yang L, Yang J (2020b) Effects of confining stresses, pre-crack inclination angles and injection rates: observations from large-scale true triaxial and hydraulic fracturing tests in laboratory. *Rock Mech Rock Eng* 53(4):1991–2000. <https://doi.org/10.1007/s00603-019-01995-2>
- Luo Q, Gong L, Qu Y, Zhang K, Zhang G, Wang S (2018) The tight oil potential of the Lucaogou Formation from the southern Junggar Basin, China. *Fuel* 234:858–871
- Ma X, Li N, Yin C, Li Y, Zou Y, Wu S, He F, Wang X, Zhou T (2017) Hydraulic fracture propagation geometry and acoustic emission interpretation: a case study of Silurian Longmaxi Formation shale in Sichuan Basin, SW China. *Pet Explor Dev* 44(6):1030–1037. [https://doi.org/10.1016/S1876-3804\(17\)30116-7](https://doi.org/10.1016/S1876-3804(17)30116-7)
- Manchanda R, Bryant EC, Bhardwaj P, Cardiff P, Sharma MM (2017) Strategies for effective stimulation of multiple perforation clusters in horizontal wells. *SPE Prod Oper* 33(03):539–556. <https://doi.org/10.2118/179126-pa>
- Manchanda R, Shrivastava K, Zheng S, Sharma M (2020) A new mechanism for the formation of hydraulic fracture swarms. In: SPE hydraulic fracturing technology conference and exhibition. Society of Petroleum Engineers
- Meglis IL, Chows TM, Young RP (1995) Progressive microcrack development in tests in Lac du Bonnet granite—I. Acoustic emission source location and velocity measurements. *Int J Rock Mech Min Sci Geomech Abstr* 32(8):741–750. [https://doi.org/10.1016/0148-9062\(95\)00014-8](https://doi.org/10.1016/0148-9062(95)00014-8)
- Ono K (2016) Calibration methods of acoustic emission sensors. *Materials* 9(7):508–508
- Petružálek M, Jechumtálová Z, Šílený J, Kolář P, Svitek T, Lokajčíček T, Turková I, Kotrlý M, Onysko R (2020) Application of the shear-tensile source model to acoustic emissions in Westerly granite. *Int J Rock Mech Min Sci*. <https://doi.org/10.1016/j.ijrmm.2020.104246>
- Ren X, Zhou L, Li H, Lu Y (2019) A three-dimensional numerical investigation of the propagation path of a two-cluster fracture system in horizontal wells. *J Pet Sci Eng* 173:1222–1235. <https://doi.org/10.1016/j.petrol.2018.10.105>
- Satoh T, Nishizawa O, Kusunose K (1990) Fault development in oshima granite under triaxial compression inferred from hypocenter distribution and focal mechanism of acoustic emission. *Sci Rep Tohoku Univ* 5(33):241–250
- Sedlak P, Hirose Y, Enoki M (2013) Acoustic emission localization in thin multi-layer plates using first-arrival determination. *Mech Syst Sig Process* 36(2):636–649. <https://doi.org/10.1016/j.ymsp.2012.11.008>
- Taghichian A, Zaman M, Devegowda D (2014) Stress shadow size and aperture of hydraulic fractures in unconventional shales. *J Pet Sci Eng* 124:209–221. <https://doi.org/10.1016/j.petrol.2014.09.034>
- Wang Y, Ju Y, Zhang H, Gong S, Song J, Li Y, Chen J (2021) Adaptive finite element-discrete element analysis for the stress shadow effects and fracture interaction behaviours in three-dimensional multistage hydrofracturing considering varying perforation cluster spaces and fracturing scenarios of horizontal wells. *Rock Mech Rock Eng* 54(4):1815–1839. <https://doi.org/10.1007/s00603-021-02364-8>
- Wu K, Olson J, Balhoff MT, Yu W (2016) Numerical analysis for promoting uniform development of simultaneous multiple-fracture propagation in horizontal wells. *SPE Prod Oper* 32(01):41–50. <https://doi.org/10.2118/174869-pa>
- Wu K, Olson JE (2015) A simplified three-dimensional displacement discontinuity method for multiple fracture simulations. *Int J Fract* 193(2):191–204. <https://doi.org/10.1007/s10704-015-0023-4>
- Wu K, Olson JE (2016) Mechanisms of simultaneous hydraulic-fracture propagation from multiple perforation clusters in horizontal wells. *SPE J* 21(03):1000–1008. <https://doi.org/10.2118/178925-pa>
- Wu M, Gao K, Liu J, Song Z, Huang X (2022) Influence of rock heterogeneity on hydraulic fracturing: a parametric study using the combined finite-discrete element method. *Int J Solids Struct* 234:111293
- Wu S, Li T, Ge H, Wang X, Li N, Zou Y (2019) Shear-tensile fractures in hydraulic fracturing network of layered shale. *J Pet Sci Eng*. <https://doi.org/10.1016/j.petrol.2019.106428>
- Xiong H, Liu S, Feng F, Liu S, Yue K (2020) Optimizing fracturing design and well spacing with complex-fracture and reservoir simulations: a Permian basin case study. *SPE Prod Oper* 35(04):703–718
- Yang Y, Ren X, Zhou L, Lu Y (2020) Numerical study on competitive propagation of multi-perforation fractures considering full hydro-mechanical coupling in fracture-pore dual systems. *J Pet Sci Eng* 191:107109. <https://doi.org/10.1016/j.petrol.2020.107109>
- Yuan L, Hou B, Li W, Xiong Z, Qin M, Chen M, Li Y (2016) Experimental investigation on fracture geometry in multi-stage fracturing

- under tri-axial stresses. In: 50th US rock mechanics/geomechanics symposium. american rock mechanics association
- Zhai H, Chang X, Wang Y, Lei X, Xui Z (2020) Analysis of acoustic emission events induced during stress unloading of a hydraulic fractured Longmaxi shale sample. *J Pet Sci Eng* 189(September 2019):106990–106990. <https://doi.org/10.1016/j.petrol.2020.106990>
- Zhang J, Tang Y, Li H (2017) STA/LTA fractal dimension algorithm of detecting the P-wave arrival. *Bull Seismol Soc Am* 108(1):230–237. <https://doi.org/10.1785/0120170099>
- Zhang S, Li S, Zou Y, Li J, Ma X, Zhang X, Zhang Z, Wu S (2021a) Experimental study on fracture height propagation during multi-stage fracturing of horizontal wells in shale oil reservoir. *J China Univ Pet (ed Nat Sci)* 45(01):77–86
- Zhang Z, Zhang S, Zou Y, Ma X, Li N, Liu L (2021b) Experimental investigation into simultaneous and sequential propagation of multiple closely spaced fractures in a horizontal well. *J Pet Sci Eng* 202:108531. <https://doi.org/10.1016/j.petrol.2021.108531>
- Zou Y, Ma X, Zhou T, Li N, Chen M, Li S, Zhang Y, Li H (2017) Hydraulic fracture growth in a layered formation based on fracturing experiments and discrete element modeling. *Rock Mech Rock Eng* 50(9):2381–2395. <https://doi.org/10.1007/s00603-017-1241-z>
- Zou Y, Zhang S, Zhou T, Zhou X, Guo T (2016) Experimental investigation into hydraulic fracture network propagation in gas shales using CT scanning technology. *Rock Mech Rock Eng* 49(1):33–45. <https://doi.org/10.1007/s00603-015-0720>

**Publisher's Note** Springer Nature remains neutral with regard to jurisdictional claims in published maps and institutional affiliations.